Design and experimental investigation of V-folded beams with acoustic black hole indentations

Nansha Gao, Zhengyu Wei, Hong Hou, et al.

Citation: The Journal of the Acoustical Society of America **145**, EL79 (2019); doi: 10.1121/1.5088027
View online: https://doi.org/10.1121/1.5088027
View Table of Contents: https://asa.scitation.org/toc/jas/145/1
Published by the Acoustical Society of America

Design and experimental investigation of V-folded beams with acoustic black hole indentations

Nansha Gao,[1,a)] Zhengyu Wei,[1] Hong Hou,[1] and Anastasiia O. Krushynska[2]

[1]*Key Laboratory of Ocean Acoustic and Sensing, School of Marine Science and Technology, Northwestern Polytechnical University, Xi'an 710072, China*
[2]*Laboratory of Bio-Inspired and Graphene Nanomechanics, Department of Civil, Environmental and Mechanical Engineering, University of Trento, Trento 38123, Italy*
gaonansha@nwpu.edu.cn, weizhengyu@mail.nwpu.edu.cn, houhong@nwpu.edu.cn, akrushynska@gmail.com

Abstract: This paper proposes a strategy to broaden complete bandgap attenuating flexural and longitudinal modes, and to shift them to lower frequencies by spatially folding designs. Numerical simulations show that the V-folded acoustic black hole beam exhibits an ultra-wide complete bandgap below 1 kHz due to longitudinal-flexural waveform transformation, and experimental results verify this finding. The proposed folded beams are easy-to-fabricate, of compact dimensions, and exhibit excellent wave attenuation functionality that makes them promising for low-frequency vibration reduction and wave attenuation applications.

[NV]
Date Received: August 20, 2018 **Date Accepted:** January 6, 2019

1. Introduction

The manipulation of low-frequency acoustic and elastic waves is a challenging scientific and engineering problem.[1,2] Substantial progress in this direction has been made after the discovery of the acoustic black hole (ABH) phenomenon.[3] The ABH allows the manipulation of flexural waves in structures, the thickness of which varies according to the power-law equation, e.g., $h(x) = \varepsilon x^m$, $m \geq 2$.[3] The tapered profile results in trapping of waves incident on an edge and does not allow them to reflect back.[4] Thus, the ABH structures have the potential to act as ideal energy absorbers.[5] Although small deviations of tapered profiles from the ideal power-law shape (i.e., inevitable truncation of a tapered edge) seriously affect the ABH effect in realistic structures, substantial energy localization at the edges can still be achieved,[6–10] for instance, by using damped materials[6] or electro-mechanical coupling,[7] by introducing multiple ABH elements,[8] or modifying the thickness profiles in different ways.[9,10]

A combination of the bandgap (BG) mechanism and the ABH phenomenon enables to extend the BG width and to design metastructures with ultra-broad BGs bounded by high-energetic modes.[11,12] In addition, only a small number of elementary units is required to achieve the low-frequency wave attenuation. Inspired by these results, we aim at a deeper understanding of the dynamics of the hybrid metastructures with the ABH indentation. Namely, we focus on developing an approach to shift BGs to lower frequencies by preserving compact structural dimensions. For this purpose, we exploit the strategy of folding the wave propagation path (i.e., beams), which has been successfully applied earlier for the design of compact acoustic wave reflectors.[1,13] In particular, we consider a set of one-dimensional beams with double-leaf ABH indentation[11,12] folded in a V-like structure. It appears that such a configuration not only allows lowering the BG frequencies for flexural waves, but also induces complete BGs to attenuate both flexural and longitudinal waves simultaneously. This is a substantial advancement as compared to the previous studies[3,5,12] focused on flexural waves only. The obtained numerical results are supported by experimental data.

2. Design, calculation, and discussion

We consider a set of periodic beams with double-leaf ABH indentation profiles [Figs. 1(a) and 1(b)] placed perpendicular to the incident wave. The beam structure is folded in a V-like configuration [Fig. 1(c)]. For clarity, we call the representative unit cells of the folded and unfolded configurations as model A and model B, respectively. The thickness of the ABH tapered profile varies as $h(x) = \varepsilon x^m (m \geq 2)$,[5] and the other

[a)]Author to whom correspondence should be addressed.

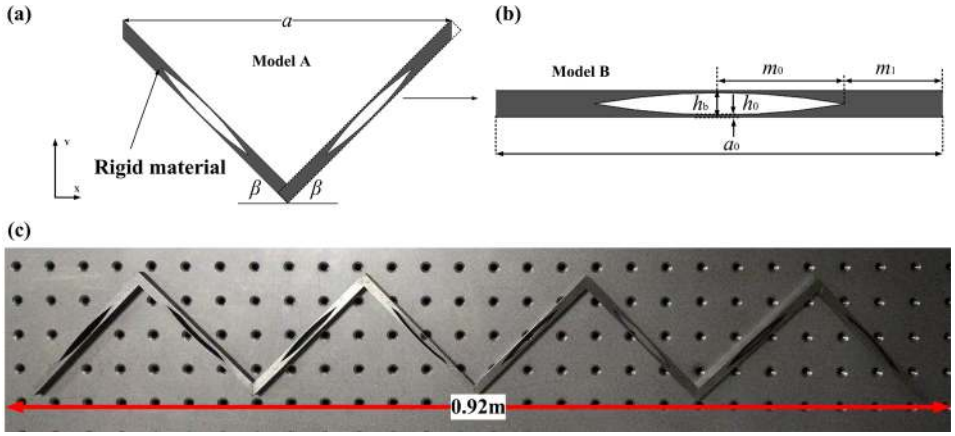

Fig. 1. (Color online) (a) Top view of the V-folded ABH beam, (b) geometric parameters of model B, and (c) top view of the experimental sample of the designed V-folded ABH beam.

relevant geometric parameters are $m_0 = m_1 = 0.03\,\text{m}$, $h_0 = 0.5\,\text{mm}$, $h_b = 6.4\,\text{mm}$, $a_0 = 0.12\,\text{m}$, and $a = 2\cos\beta(a_0 - h_b) \approx 0.23\,\text{m}$. The total length of the finite-size structure composed of four model A units is 1 m.

As shown in Refs. 11 and 12, the periodically arranged model B can produce an ultra-broad BG for flexural waves. However, in the V-folded configurations (model A), flexural waves are coupled to longitudinal waves due to reflections at the beam joints, and thus it is impossible to distinguish these two mode types. Hence, in this work, in contrast to the other works on beams with ABH indentation,[3,5,12] we focus on the generation and analysis of complete BGs for flexural and longitudinal modes. The wave dispersion in the designed structures is evaluated numerically by using the Structural Mechanics Module in COMSOL Multiphysics 5.3. For this purpose, we apply Floquet–Bloch boundary conditions at the lateral boundaries. The dispersion curves can be obtained by sweeping a wave vector along the first Brillouin zone. Since the V-folded ABH beam is periodic along one dimension, the first Brillouin zone is a straight line with the reduced non-dimensional wavenumber varying from 0 to 1.[2] The calculated dispersion diagrams are shown in Fig. 2 for Nylon (Young's modulus 2 GPa, Poisson's ratio 0.4, and mass density 1150 kg/m^3) and structural steel (Young's

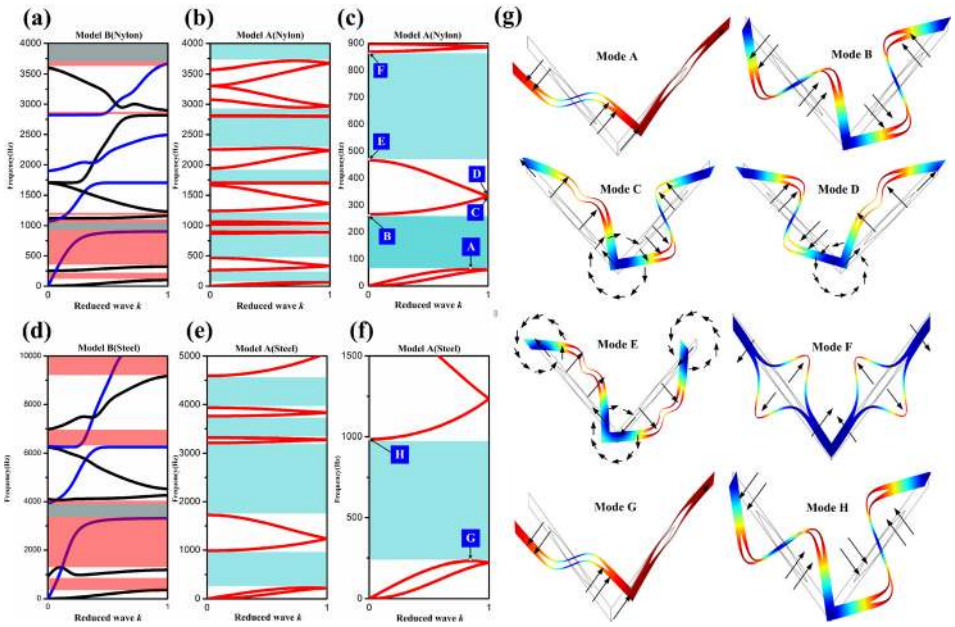

Fig. 2. (Color online) (a)–(f) Band structures of models A and B made of nylon and steel, respectively. Pale pink and blue areas correspond to flexural and complete BGs, respectively; red curves indicate dispersion branches of model A; blue and black curves indicate longitudinal and flexural modes of model B, respectively. Points A–G are the boundary points distributed on the lower and upper BG of model A. (g) Vibration modes marked in (c) and (f) with a black arrow indicating vibration direction. Here red indicates maximum displacements, while blue indicates minimum displacements.

modulus 205 GPa, Poisson's ratio 0.28, and mass density 7850 kg/m^3). Figures 2(a) and 2(d) present diagrams for the unfolded structures (model B) with black and blue curves indicating uncoupled flexural and longitudinal modes. The BGs for flexural and all mode types are highlighted in pale magenta and gray, respectively. Band structure diagrams for the V-folded structure (model A) are shown in Figs. 2(b), 2(c), 2(e), and 2(f), where complete BGs for all mode types are shaded in light blue.

In Fig. 2(a), the dispersion diagrams for model B exhibits five BGs for flexural modes and two complete BGs at the considered frequencies. Note that the material properties significantly affect the BG width and frequencies of the BGs, while the dispersion curve trends remain almost unchanged. Namely, by selecting a more rigid material for the beams (steel), it is possible to shift the BGs to higher frequencies by simultaneously increasing the BG width. This behavior can be explained by a higher impedance mismatch between the air and steel as compared to Nylon. The same dependence on material properties is observed for the V-folded structure (model A). For instance, there are eight complete BGs with the lowest two below 900 Hz for Nylon structure [Figs. 2(b) and 2(c)]. For steel [Figs. 2(e) and 2(f)], only four of these BGs occur in the analyzed frequency range and have a much wider BG width, while the other four are shifted to higher frequencies. In general, the induced BGs in model A have lower frequencies than those in model B {compare complete BGs Figs. 2(a) [Fig. 2(d)] and Fig. 2(c) [Fig. 2(f)]} due to the enlargement of the unit cell size from the folding.[13] In particular, the lowest ultra-broad BG for the steel structure is below 1 kHz [Fig. 2(f)] with the BG width of 718 Hz and the mid-BG frequency 608 Hz, that can be attractive for low-frequency vibration control and noise reduction. The bandwidth of the second BG [Fig. 2(e)] reaches 1469 Hz. The BGs in the Nylon V-folded structure occur at even lower frequencies (e.g., the first BG is between 100 and 300 Hz), but the limited BG width is undesirable for vibration mitigation applications.

The analysis of the vibration modes brings further insight into the physical mechanisms of the BG generation process. Here we analyze vibration patterns for model A only, since the detailed analysis of model B has been performed previously elsewhere (e.g., in Refs. 11 and 12). As the trends of dispersion curves are insensitive to the choice of a structural material, the vibration patterns corresponding to similar modes should also be identical. It is indeed the case, as follows from the comparison of modes bounding the lowest BG [see Fig. 2(g), points A and G, points B and H].

The mode at the lower bound of the first BG [Fig. 2(g), points A and G] is characterized by anti-symmetric flexural vibrations of the left-hand side of the unit cell and longitudinal extensions of the right-hand side. Such a pattern indicates the coupling between two different types of modes in the V-folded structure. Indeed, the comparison of the corresponding dispersion curves in Figs. 2(a) and 2(b) reveals that the lower BG bound in model A originates from the coupling of independent flexural and longitudinal modes in model B. This "longitudinal-flexural" waveform transformation unfolds the first complete BG in the V-folded ABH beam. At the upper BG bound [Fig. 2(g), modes B and H], the two beams vibrate in-phase, and the maximum flexural deformation is concentrated in the ABH region that perfectly agrees with the flexural nature of this mode. The next two modes [Fig. 2(g), modes C and D], are characterized by flexural vibrations of a unit-cell half, and mixed longitudinal and out-of-plane "double-crest" vibrations of another half. In addition there occurs a rotating vibration relative to the folding tip (clockwise for mode C, and counter-clockwise for mode D) caused by different vibration types at the two sides. Note that this type of specific distribution of the vibration energy does not allow generating a BG between the modes C and D.

At the lower bound of the second BG [mode E in Fig. 2(g)], the mode shape is characterized by symmetric in-plane longitudinal vibrations accompanied by two out-of-plane double-crest vibrations and three rotating vibrations (of which two are counter clockwise and the other is clockwise). In the double crest vibrations, the deformation energy is concentrated near the two crests of the ABH beams, similar to the effect of local resonance. The ABH indentation thus acts as continuously distributed local resonators with multiple degrees of freedom that leads to broadband BGs[12] of a different nature as compared to typical locally resonant BGs.[14] Finally, the upper bound of the second BG is characterized by symmetric flexural vibration of the two unit-cell parts, and thus, the longitudinal-flexural waveform transformation is preserved.

The described variety of the vibration patterns in the V-folded beams with ABH indentation (model A) results in a larger number of low-frequency BGs as compared to the unfolded counterpart (model B). Therefore, the folding not only results in

the mode coupling, but also brings additional degrees of freedom to the system, such as rotational motions, that enriches the system dynamics and allows extending its attenuation abilities to lower frequencies.

3. Experimental verification

Experiments were conducted to further validate the vibration attenuation effect of the V-folded ABH beam. The sample is shown in Fig. 1(c); its matrix material adopts No. 20 structural steel (numbering designation: U 20252), its mass density of 7749 kg/m^3 and Young's modulus of 200 GPa are close to the material attribute setting in finite element analysis. We use laser cutting machine (MARVEL 6000) to fabricate the experimental samples consisting of four periodic units. Thin lines are used to lift the whole sample horizontally to mimic free vibration. The electromagnetic vibration excitation is used as the input source, and the flexural and longitudinal exciting points are set to be on the left side of the sample. A laser scanning vibrometer is used for vibration pickup on the right side. $20\log w_{out}/w_{in}$ (w_{out} and w_{in} are the output and input of displacement, respectively) are defined to depict the attenuation of vibration. At the input end of the vibration, the laser scanning vibrator could pick up the vibration displacement of the flexural wave excited by the electromagnetic vibration exciter directly, but for longitudinal vibration, the placement position of the electromagnetic vibrator would block the laser irradiation, so the longitudinal vibration pickup point of the input end is set to be on the folding tip region of the leftmost unit structure, as shown in Fig. 3(a). The electromagnetic vibration exciter, fed by power amplifier B&K 2732, produces a periodic chirp signal (10–3000 Hz), and the multichannel analyzer B&K 3560C turns the pickup signal into the B&K 4809 Pulse, then the time domain signals obtained by the laser scanning vibrometer (Polytec PDV-100) are alternated by fast Fourier transform; the results are exhibited in Fig. 3(d).

Below 3000 Hz, the sample has a strong attenuation on flexural and longitudinal vibration in the first two complete BGs, and absorption of the flexural wave is more significant. In the first complete BG, most of the flexural wave transmissions are lower than −40 dB, and in the second one, the lowest point of the transmission could reach −80 dB. Longitudinal vibration attenuation by this sample is not obvious like the flexural wave; the reason is that the longitudinal pickup point is not the exciting point for the input end, hence, input of displacement w_{in} would not be very accurate for describing the real physical characteristics, but their transmissions are still basically lower than −20 dB, which can be considered to reach the vibration reduction standard in engineering. The BG regions agree well with the low ebb of transmission in the vibration experiment, and prove that the finite structure designed in this work can attenuate both the flexural and longitudinal waves. We note that there appear several

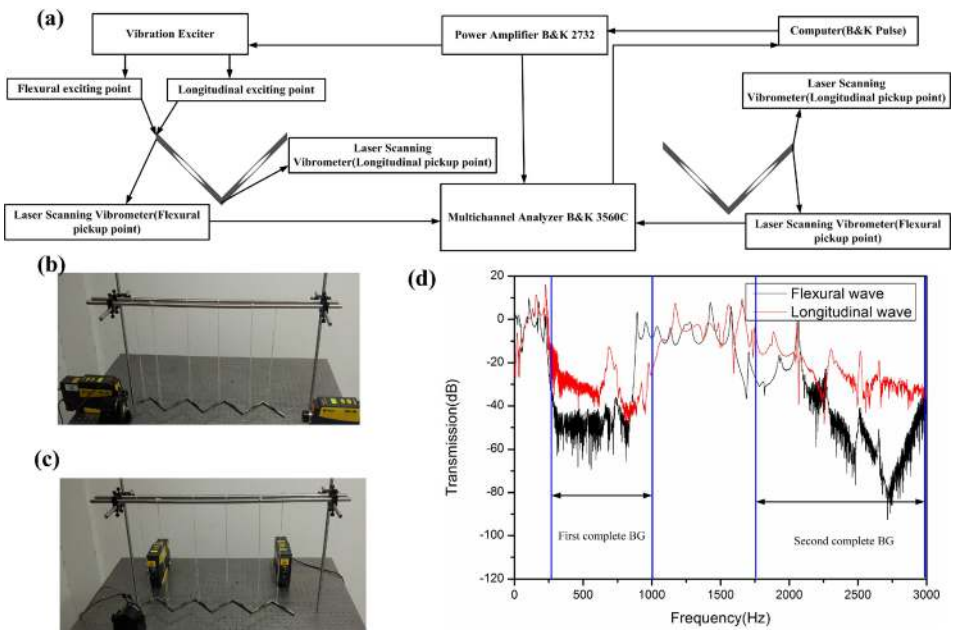

Fig. 3. (Color online) (a) Schematic diagram of the experimental setup with excitation and acquisition points for longitudinal and flexural waves shown separately. [(b) and (c)] Photos of the experimental setup. (d) Transmission of flexural and longitudinal waves in model A made of steel: areas between the blue lines correspond to complete BGs shown in Figs. 2(e) and 2(f).

resonance peaks in Fig. 3(d) at the frequencies of the first and second complete BGs. One of the reasons for the occurrence of these peaks is the finite size of the sample, which is not taken into account in the dispersion analysis. Another reason is the interaction of incident and reflected waves at the free boundaries causing localized surface states. The fluctuation in the experimental data curve originates from the rotational mode and the excitation force on the central axis in the ABH beam. In addition, the sample length is up to 0.92 m and the laser process temperature is very high; the slender beam would be deformed because of the uneven heat, which leads to the sample distortion, so the experimental data curve is not smooth.

4. Conclusions

In summary, we have proposed to exploit structural folding to lower BG frequencies in ABH beams. We have demonstrated numerically and experimentally that the V-folded ABH beams can efficiently attenuate all types of elastic waves, including longitudinal modes that distinguish them from the other previously analyzed ABH structures. We have also shown that the host material properties influence the wave attenuation performance and allow one to induce BGs at different frequencies. The key effects of the spatial folding are: (1) the activation of the waveform transformation mechanism responsible for the formation of complete BGs for flexural and longitudinal waves, (2) the enrichment of the structural dynamics due to the added effects of rotations, and (3) the reduction of the structural length that might be advantageous for practical configurations. The performed experiments validate the numerical results and confirm that a few unit cells are sufficient to efficiently attenuate all types of propagating elastic waves. Thus, the excellent wave attenuation performance and easy-to-fabricate design for the proposed ABH metastructures open bright perspectives for multiple engineering applications in the field of low-frequency wave manipulation and vibration control.

Acknowledgments

This work was supported by the National Natural Science Foundation of China (Grant Nos. 11704314 and 11474230), China Postdoctoral Science Foundation Funded Project (Grant No. 2018M631194), and National Key Research and Development Program of China (Grant No. 2016YFF0200902) for financial support. We thank Professor Joo Hwan Oh of Ulsan National Institute of Science and Technology for the effective academic discussion.

References and links

[1]A. O. Krushynska, F. Bosia, M. Miniaci, and N. M. Pugno, "Spider web-structured labyrinthine acoustic metamaterials for low-frequency sound control," New J. Phys. **19**(10), 105001 (2017).
[2]N. Gao, H. Hou, J. H. Wu, and B. Cheng, "Low frequency band gaps below 10 Hz in radial flexible elastic metamaterial plate," J. Phys. D: Appl. Phys. **49**, 435501 (2016).
[3]V. V. Krylov, "On the velocities of localized vibration modes in immersed solid wedges," J. Acoust. Soc. Am. **103**, 767–770 (1998).
[4]V. V. Krylov, "New type of vibration dampers utilising the effect of acoustic 'black holes'," Acta. Acust. Acust. **90**(5), 830–837 (2004).
[5]L. Zhao, "Passive vibration control based on embedded acoustic black holes," J. Vib. Acoust. **138**, 041002 (2016).
[6]C. C. Stephen and A. F. Philip, "Progressive phase trends in plates with embedded acoustic black holes," J. Acoust. Soc. Am. **143**, 921–930 (2018).
[7]L. Zhao, C. C. Stephen, and F. Semperlotti, "Broadband energy harvesting using acoustic black hole structural tailoring," Smart Mater. Struct. **23**, 065021 (2014).
[8]P. A. Feurtado and S. C. Conlon, "Transmission loss of plates with embedded acoustic black holes," J. Acoust. Soc. Am. **142**, 1390–1398 (2017).
[9]L. Tang and L. Cheng, "Enhance acoustic black hole effect in beams with a modified thickness profile and extended platform," J. Sound. Vib. **388**, 42–52 (2017).
[10]P. A. Feurtado, S. C. Conlon, and F. Semperlotti, "A normalized wave number variation parameter for acoustic black hole design," J. Acoust. Soc. Am. **136**, EL148–EL152 (2014).
[11]T. Zhou, L. Tang, H. Ji, J. Qiu, and L. Cheng, "Dynamic and static properties of double layered compound acoustic black hole structures," Int. J. Appl. Mech. **9**, 1750074 (2017).
[12]L. Tang and L. Cheng, "Ultrawide band gaps in beams with double-leaf acoustic black hole indentations," J. Acoust. Soc. Am. **142**, 2802–2807(2017).
[13]A. O. Krushynska, F. Bosia, and N. M. Pugno, "Labyrinthine acoustic metamaterials with space-coiling channels for low-frequency sound control," Acta. Acust. Acust. **104**, 200–210 (2018).
[14]N. Kaina, M. Fink, and G. Lerosey, "Composite media mixing Bragg and local resonances for highly attenuating and broad bandgaps," Sci. Rep. **3**, 3240 (2013).